

A comparative study of the vibrational and luminescence properties of embedded Ge nanocrystals prepared by ion implantation and sputter deposition methods: role of strain and defects

P K Giri^{1,2}, S Bhattacharyya¹, Kaustuv Das³, S K Roy³,
R Kesavamoorthy⁴, B K Panigrahi⁴ and K G M Nair⁴

¹ Department of Physics, Indian Institute of Technology Guwahati, Guwahati 781 039, India

² Centre for Nanotechnology, Indian Institute of Technology Guwahati, Guwahati 781 039, India

³ Department of Physics and Meteorology, Indian Institute of Technology Kharagpur, Kharagpur 721 302, India

⁴ Materials Science Division, Indira Gandhi Center for Atomic Research, Kalpakkam 603 102, India

Received 29 June 2007, in final form 4 October 2007

Published DD MMM 2007

Online at stacks.iop.org/SST/22/1

Abstract

We present a comparative study of the vibrational and luminescent properties of Ge nanocrystals (NCs) prepared by two different techniques, namely ion implantation (process I) and radio frequency (RF) sputter deposition technique (process II). Ge NCs of size 6–13 nm are formed embedded in a SiO_x matrix as a result of post-deposition annealing. Optical Raman studies reveal the presence of strain in the embedded Ge NCs in both cases. Polarization dependent low frequency Raman scattering studies show that process I yields NCs with surface symmetrical Raman modes only, whereas process II yields additional surface quadrupolar Raman modes. Photoluminescence (PL) studies using 488 nm excitation show a broad emission band that can be deconvoluted into two peaks centered at ~535 nm and ~594 nm. PL studies on Ar implanted and similarly annealed SiO_x layers confirm that the 535 nm and 594 nm emission bands are originated from oxygen deficient defects (ODCs) in the SiO_x matrix. PL studies with 325 nm excitation show additional strong peaks in the ultraviolet-blue region. Analyses of the PL spectra from various samples show that different PL emission bands are related to various forms of ODCs having different environments dependent on different defect formation processes. It is concluded that due to poor quality of interface between NC and defective SiO_x matrix, recombination at defects dominates the room temperature light emission from embedded Ge NCs, while light emission due to quantum-confined carriers in the NCs is quenched, perhaps due to inherent strain in the embedded NCs.

1. Introduction

In recent years, there is an upsurge of interest to understand the optical properties of Ge nanocrystals (NCs) in the quantum

confinement regime, since these NCs appear to have promising light emitting and charge storage characteristics. However, a proper correlation between the structure and optical properties of Ge NCs has rarely been found experimentally. Furthermore,

intriguing role of defects and effect of electron and phonon confinements are poorly understood in Ge NCs as compared to their counterpart in Si NCs. Experimental observations have rarely met the theoretical predictions regarding the superior optical properties of Ge NCs. Several studies have indicated that the defects in the surrounding matrix are primarily responsible for broad photoluminescence (PL) in the visible region [1, 2], while some studies attribute the luminescence to quantum confinement of charge carriers in the NCs [3, 4]. Recently, a hybrid model has been proposed to account for the visible PL from embedded Ge NCs prepared by two different techniques [5]. Torchynska *et al* have shown that in Ge or Si-rich Si oxide film, the visible PL in the range of 1.7–1.8 eV and 2.0–2.3 eV are related to defects at Si/SiO_x interface and silicon suboxide, respectively [6]. On the other hand, Das *et al* have attributed the 1.7–1.8 eV broad emission to recombination at Ge NCs with a size distribution [7]. In some cases, an orange PL band at 1.9 eV has been assigned to substoichiometric Ge oxide (GeO_x) [8]. Rebohle *et al* [9] reported a strong blue-violet PL and electroluminescence from Ge-implanted and Si-implanted SiO₂ layers, and they attributed the observed PL to neutral oxygen vacancies in SiO₂ [10]. Similarly, Sahoo *et al* observed stable violet emission from Ge-implanted α -quartz and attributed it to Ge-related defects [11]. On the other hand, Liao *et al* [12] and Feinardi and Paleari [13] observed violet PL in SiO₂ samples that does not contain Ge atoms and the violet emission was attributed to oxygen deficient defects (ODCs) in SiO₂. Infrared PL has also been attributed to defect states in the NCs [2]. Most of these studies have been carried out on samples prepared by a single technique. A comprehensive understanding of mechanism of light emission from embedded Ge NCs is feasible with comparative studies on samples prepared by different techniques. Furthermore, most of the reported studies have been performed with visible light excitation (488 nm or 459 nm light sources) that give only a partial picture of the density of states taking part in the luminescence process and very few studies have been carried out with UV excitation [9, 12–14].

For ultrasmall Ge NCs, structural transformation has been proposed in the literature to account for the visible PL [15]. Distinct signature of structural disorder in Ge NCs grown by ion implantation in silica has been reported [16]. Presence of compressive stress on embedded Ge NCs has been studied by several groups [17–19]. Sharp *et al* [20] have recently made *in situ* TEM observation of growth of sapphire-embedded Ge NCs and found a compressive stress of 3–5 GPa on the embedded Ge NCs. However, the implications of strain on the optical properties of NCs are least explored in the literature. Despite the evidence of well-characterized Ge NCs prepared by different methods such as ion implantation, sputtering etc, unambiguous evidence for the excitonic emission from quantum-confined carriers in Ge NCs is lacking in the literature. Thus, it is imperative to understand the specific role of defects and lattice strain in the NCs on the photoluminescence properties of embedded Ge NCs. It is anticipated that in addition to the defects at the NC surface and defects in the embedding matrix, strain in the NCs may adversely influence the light-emitting properties of Ge NCs.

Raman scattering is a powerful tool to understand the structural properties of NCs. Raman studies have been

utilized to monitor stress in Ge NCs embedded in silicon oxide [16–19]. Low frequency Raman scattering (LFRS) has proved to be a powerful tool to monitor surface vibrational modes of embedded NCs [21]. While the optical Raman spectra of Ge NCs of different sizes have been reported [19, 22], distinctive features of Raman modes dominated by surface atoms and those dominated by interior atoms are less studied. In the low-frequency range, Raman modes whose frequencies increase with decrease in NC size have been reported for various metals [23] and semiconductors [21, 24], and were attributed to the distortion modes of a continuum sphere [25]. Theoretically predicted low frequency surface vibrational modes for Ge NCs [26] have been verified for Ge NCs prepared by the ion-implantation technique [27]. However, sputter-deposited Ge NCs have not been studied much. Very recently, Yang *et al* have reported acoustic phonon modes of embedded Ge NCs [28]. Experimental determination of the low-frequency modes is often difficult for small NCs, since the scattering cross-section is quite low for small sized NCs, whereas for the larger size NCs low-frequency modes fall in a region where the Rayleigh tail dominates the scattering intensity.

In this work, we have studied the light emitting and vibrational properties of embedded Ge NCs prepared by RF sputtering and ion-implantation techniques. Ge NCs embedded in a SiO₂ matrix are characterized by x-ray diffraction (XRD), transmission electron microscopy (TEM), Raman and photoluminescence (PL) spectroscopic techniques. Origin of the visible and strong UV PL emission at room temperature is discussed in the light of the strain and defects present in the matrix as well as surface/interface of the NCs. Possible mechanism of quenching of expected PL emission from Ge NCs is also discussed.

2. Experimental details

The Ge–SiO₂ thin films were deposited on (100) oriented p-type Si substrates by RF magnetron co-sputtering (process I). Prior to the deposition, the Si substrates were dipped in dilute hydrofluoric acid to remove the surface native oxide followed by rinsing in de-ionized water and drying in a flux of N₂. The target used was a 3 inch n-type Si wafer masked with Ge wafer pieces of defined area. The chamber was first evacuated to a base pressure of 1×10^{-6} Torr. The target-to-substrate distance was kept fixed at 6 cm and the working pressure was maintained at 0.11 Torr by introducing oxygen and argon in the ratio of 2:1. The depositions were carried out at a RF power 50 W for 1 h. No external heating of the substrate was employed during deposition. Both sputtered Si and Ge species while transporting through the oxygen discharge become oxidized and condense on the substrate. As-deposited samples are subsequently annealed at 700 °C (Sp1) and 900 °C (Sp2) for 1 h in nitrogen ambient to grow Ge NCs of various sizes. Since Ge is thermodynamically less stable in its oxide form than Si, GeO_x may be reduced to Ge under high temperature annealing. Annealed samples were studied by XRD, TEM, PL and optical Raman and low-frequency Raman scattering (LFRS) measurements.

In the ion-implantation method (process II), 300 keV Ge⁺ ions were implanted at room temperature on thermally grown (wet-oxidation) SiO₂ films of thickness \sim 300 nm on a Si(100)

Table 1. Details of the samples used in this work.

Preparation method	Deposition time/ Ge ⁺ dose (cm ⁻²)	Annealing temperature	Sample name	Average size of Ge NCs (nm)
RF sputtering	1 h	700 °C	Sp1	7.3
RF sputtering	1 h	900 °C	Sp2	9.1
Ge ⁺ implanted in SiO ₂	3 × 10 ¹⁶	950 °C	Ge1	6.1
Ge ⁺ implanted in SiO ₂	1 × 10 ¹⁷	950 °C	Ge2	13.0
Ar ⁺ implanted in SiO ₂	5 × 10 ¹⁶	900 °C	Ar1	–

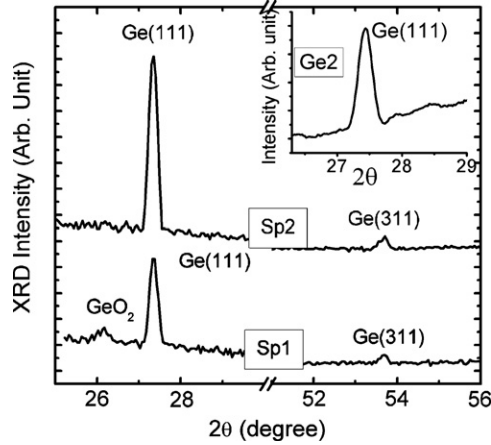


Figure 1. XRD pattern for Sp1, Sp2 and Ge2 samples showing formation of (1 1 1) and (3 1 1) oriented Ge NCs. Sp1 shows presence of GeO₂ phase due to lower temperature of annealing.

substrate with fluences 3 × 10¹⁶ (Ge1) and 1 × 10¹⁷ (Ge2) ions cm⁻². Implanted and unimplanted SiO₂ layers were first heat treated at 800 °C for 1 h and further treated at 950 °C for 2 h in argon gas ambient. Evolution of the Ge NCs has been studied after each step of annealing by using XRD, PL, Raman and LFRS techniques. For comparison, Ar ion is implanted (dose: 5 × 10¹⁶ cm⁻²) on a thermally grown SiO₂ layer and annealed at 900 °C to study PL emission caused by defects in the SiO₂ layer. This sample will be referred to as Ar1 for further discussion. For the ease of discussion, the details of the samples with nomenclature are presented in table 1.

XRD measurements were performed in a grazing incidence mode using a Powder diffractometer (Bruker D8 Advance) with a thin-film mode attachment. The TEM observations were carried out using a JEM 3000 F field emission microscope with an operating voltage of 300 kV. Raman spectra for all the samples were recorded in the backscattering geometry using a vertically polarized 488 nm argon-ion laser. Low frequency Raman spectra were recorded from 5 to 40 cm⁻¹ at steps of 0.5 cm⁻¹ using the same setup. Steady-state PL measurements were made with two different laser excitations: 325 nm (He–Cd laser) and 488 nm (Ar ion laser) at room temperature, using a Jobin-Yvon T64000 spectrometer equipped with a cooled charged coupled detector.

3. Results and discussion

3.1. XRD and TEM studies

Figure 1 shows the XRD pattern for samples Sp1 and Sp2, and the inset shows the pattern for sample Ge2. Peaks at

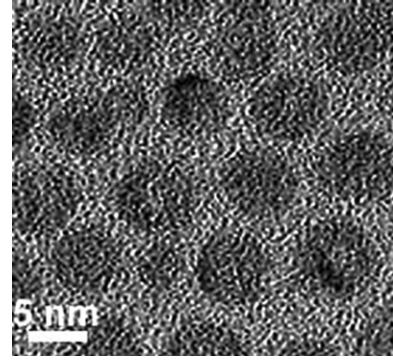


Figure 2. A typical high resolution TEM image of Ge NCs (dark regions) embedded in the SiO₂ matrix (background) for sample Sp2. Spherical NCs of size 7–8 nm are clearly seen.

27.3° and 53.7° are signature of Ge NCs grown with (1 1 1) and (3 1 1) orientations, respectively. In a low temperature annealed sample, the presence of GeO₂ along with Ge NCs is clear from the figure. At higher temperature of annealing (≥900 °C), the Ge(1 1 1) related peak dominates the spectra. Figure 2 shows a typical TEM image (high resolution) of the embedded Ge NCs in sample Sp2. Embedded Ge NCs (dark spheres) are found to be evenly distributed in the SiO₂ matrix and apparently uniform in size (7–8 nm) with a nearly spherical shape. In Sp1, the average size of the Ge NCs is expected to be smaller due to lower temperature of annealing. For different samples, the average size of the NCs was estimated from LFRS measurements and compared with the TEM results.

3.2. Optical Raman and low frequency Raman scattering studies

Figure 3 shows typical optical Raman spectra for the Sp2 sample showing a 300.9 cm⁻¹ peak due to Ge–Ge modes and a 420 cm⁻¹ peak due to localized Si–Si motion in the neighborhood of one or more Ge atoms in the SiO_x matrix [29]. In all the samples, the Raman line width for the Ge–Ge peak is found to be relatively broad (e.g. ~20 cm⁻¹ in Sp2) as compared to the bulk Ge crystal Raman line width (~4 cm⁻¹). The Raman spectrum of the Ge1 sample shown in the inset of figure 3 shows a line width of ~15 cm⁻¹. The line width broadening is primarily caused by confinement of phonons in the Ge NCs. Raman line width is known to be inversely proportional to the size of the NCs.

In order to describe quantitatively the Raman spectra, the standard phonon confinement model [30] can be adopted to estimate the mean size d of Ge NCs. For spherical NCs (as found in our samples), the first-order Raman spectrum $I(\omega)$ is

$$I(\omega) \propto \int \exp(-q^2 d^2/4) d^3 q / \{[\omega_0 - \omega(q)]^2 + (\Gamma/2)^2\}, \quad (1)$$

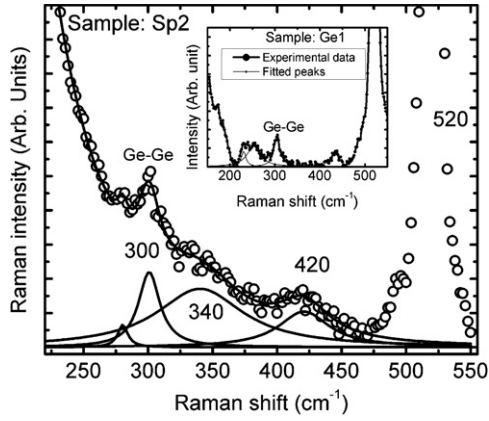


Figure 3. An optical Raman spectrum of Sp2 showing Ge–Ge modes (300.9 cm^{-1} with an FWHM = 20 cm^{-1}) corresponding to the formation of Ge NCs. Experimental spectra (symbols) are fitted with Lorentzian line shapes (solid lines). The inset shows the Raman spectra of Ge1 showing presence of Ge NCs.

where $\omega_0 = 300.4 \text{ cm}^{-1}$; q is expressed in units of $2\pi/a_{\text{Ge}}$, with $a_{\text{Ge}} = 0.565 \text{ nm}$ being the lattice constant of Ge. Γ is the natural line width ($\approx 3.5 \text{ cm}^{-1}$) and $\omega(q)$ is the dispersion relation for optical phonons in c-Ge. Since the crystallite size d is larger than the lattice constant a_{Ge} , we may take $\omega(q) = [A + B \cos(\pi q/2)]^{1/2}$, where $A = 1.578 \times 10^5 \text{ cm}^{-2}$ and $B = 1.000 \times 10^5 \text{ cm}^{-2}$ [19]. Using the above equation, we calculate the Raman intensity profile to obtain the mean crystallite size. Note that we expect a downshift of the Raman peak position due to the small crystallite size, which is contrary to the observation of small **up shift** ($\sim 0.5 \text{ cm}^{-1}$) of the peak. In the Raman spectra of the Sp2 sample, the observed FWHM of 20 cm^{-1} for the 300.9 cm^{-1} peak would correspond to an average NC size of $d = 4.6 \text{ nm}$, as predicted from equation (1). However, the mean sizes of the NCs as determined from TEM and LFRS studies (shown later) are about double of this size. Interestingly, equation (1) predicts that a crystallite size of 7–8 nm would give rise to a FWHM of 9–11 cm^{-1} , in contrast to the observed FWHM of 20 cm^{-1} . Hence, the additional line width and the observed up shift of 300.4 cm^{-1} peak must be contributed by other factors such as strain in these small crystallites. The compressive stress exerted on Ge NCs may increase with decreasing crystallite size [19], because the Ge NCs are embedded in the SiO_2 matrix. The nearest-neighbor distance in $\alpha\text{-SiO}_2$ is of the order of 0.16 nm and that in Ge crystals is 0.24 nm. The mismatch will result in a compressive stress on the Ge NCs. The stress causes an upward shift of the c-Ge peak, thereby compensating the downward shift caused by the confinement on phonon frequency. According to the calculation of Wu *et al* [19], for the NC size of 7–8 nm, we expect a downshift of Raman peak frequency by $\sim 3 \text{ cm}^{-1}$. The compressive stress s can be estimated from this downshift ($\Delta\omega$) using a formula $\Delta\omega = -s(P + 2Q)/2\omega_c$, where $P = -1.3\omega_c^2$ and $Q = -1.65\omega_c^2$ are the phonon deformation potentials of Ge, and ω_c is the frequency of the Ge crystalline peak [19]. Since our TEM studies do not show any significant distribution in NC sizes, we neglect the contribution of particle size distribution to Raman line shape and estimate a compressive stress of 0.34% for the Ge NCs present in sample Sp2. This stress is primarily

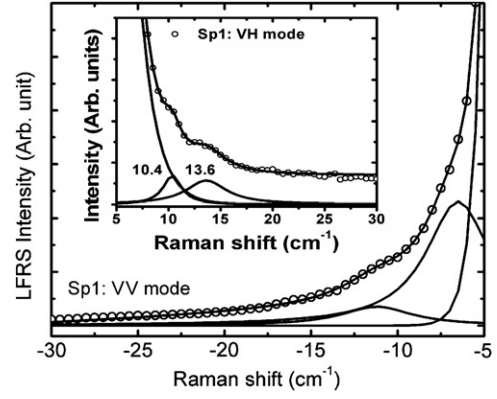


Figure 4. LFRS spectra of Sp1 in VV mode of polarization showing peaks for NCs. The inset shows LFRS spectra recorded in VH mode of polarization. Lorentzian line shapes (solid line) are fitted to the experimental spectra (symbols). Two peaks are due to surface symmetrical and surface quadrupolar modes of vibration of a NC.

responsible for the up shift of Raman peak and the additional broadening in line width of Raman spectra. In sample Sp1, the compressive stress would be relatively large since the NC sizes are expected to be smaller; as a result, the Raman signal is very weak and broad. Broad Raman spectra from sputter-deposited Ge have been reported by Das *et al* [31] and have been attributed to the size distribution and the strain in the deposited film without any quantitative analysis. However, several studies have clearly indicated the presence of strain in the SiO_2 -embedded Ge NCs [17–20]. There could be various sources of strain in embedded Ge NCs: (i) liquid–solid phase transition in Ge during a high-temperature heat treatment, (ii) lattice mismatch between the Ge and SiO_2 matrix, and lattice mismatch between Si and Ge, (iii) composition of the surrounding oxide matrix such as silicon suboxide (SiO_x) or Ge suboxides (GeO_x), and (iv) imperfect surface reconstruction during growth of NCs. Using Rutherford back scattering spectrometry, we have found that in ion-implanted samples, the surrounding matrix of NCs has a composition of SiO_x ($x \sim 1.78$). Similarly, the compositions of GeO_x and SiO_x are sensitive to the processing temperature and partial pressure of oxygen during sputter deposition. In fact, our Raman results show that for the Sp1 sample the Si–Ge peak is at 445 cm^{-1} (not shown), whereas in the Sp2 sample the Si–Ge peak is located at 420 cm^{-1} . This indicates that in the Sp2 sample, some of the Si–Si motions are replaced by Si–Ge bonds [29] as a result of higher temperature annealing, as compared to the Sp1 sample. Lopes *et al* found that in Ge-implanted SiO_2 , even after 900°C annealing, a significant fraction of up to $\sim 20\%$ of the Ge content still remain distributed in the oxide matrix around the NCs [32]. Hence, these factors contribute to the strain and the present Raman results confirm the presence of strain in Ge NCs. Our results are consistent with previous reports on strain in embedded Ge NCs [17–20].

Figure 4 shows LFRS spectra for Sp1 recorded under VV polarization geometry. The inset shows the spectra recorded under VH geometry. In both cases, two distinct peaks are observed. It has been shown that spheroidal modes with $l = 0, 2$ are Raman active and torsional modes are Raman inactive [21]. The surface quadrupolar mode ($l = 2$) appears in both polarized and depolarized geometry, whereas the surface

symmetrical mode ($l = 0$) appears only in the polarized geometry. In the present study, since the LFRS peaks appear in both VV and VH geometry, we assign the lower frequency mode to surface symmetrical (0, 0) and the higher frequency mode to surface quadrupolar (0, 2) modes of confined acoustic phonons, as per the standard notation to denote a phonon mode [21]. Similar LFRS modes have been reported recently for ZnO nanocrystals [33]. From the measured low frequency modes in Sp1, the NC sizes are calculated as 7.3 nm using the standard formula for the spheroidal mode in Ge NCs [34]: $\nu_0^S = 0.7 \frac{v_t}{dc}$ ($n = 0$), where c is the velocity of light, d is the average diameter of the NCs, and v_t is the transverse velocity of sound in Ge NCs. We have assumed a $v_t = 3.25 \times 10^5$ cm s⁻¹ for Ge [33]. In the Sp2 sample, the corresponding sizes grow to 9.1 nm as estimated from the LFRS peak, due to the higher temperature annealing. The sizes reported in table 1 are based on the LFRS analyses on Sp1, Sp2, Ge1 and Ge2 [27]. The estimated sizes are in close agreement with the size observed from TEM measurements. Any deviation in the results would be expected for non-spherical shape of the NCs and assumption of appropriate boundary conditions. Therefore, measurement of acoustic phonon modes allows a fair assessment of the size and shape of the NCs and thus it is a powerful nondestructive technique to characterize nanocrystals. Note that in the Ge1 and Ge2 samples, we observed LFRS peaks only in a VV configuration [27], and the peaks are attributed to the surface symmetrical (0, 0) spheroidal mode. This is in contrast to the case of Sp1 and Sp2 samples, where we observe both symmetrical (0, 0) mode and quadrupolar (0, 2) mode. This is believed to be due to different surrounding of the NCs prepared by two different methods. In these two cases, the Ge/SiO₂ interface is expected to be different due to different processing conditions. In the case of ion implantation method, the lattice-damage-induced strain in the SiO₂ matrix may be forbidding the surface quadrupolar mode to be observed.

3.3. Photoluminescence studies

In Ge-implanted samples, the nature of PL emission with 488 nm excitation has been previously reported by us [35]. In this section, we compare the PL results of samples prepared by process I and process II with that of sample Ar1. Figure 5 shows the room temperature PL spectra of Ar1, Ge2, Sp1 and Sp2 samples with a laser excitation of 488 nm. All the samples including Ar1 show a broad feature in PL in the visible region of wavelength. The sputter-deposited samples show low intensity emission and the ion-implanted samples show a relatively stronger emission band constituting two peaks centered at ~ 535 nm and ~ 594 nm. Samples prepared by both process I and process II do not show any significant size dependence in PL emission energy [29]. Since the peak position is almost independent of the size of the NCs and the implantation species, the related emission cannot be ascribed to the radiative recombination of excitons confined in the Ge NCs. The emission band should be related to defects in the SiO_x matrix. In the literature, similar peaks at ~ 540 nm are attributed defects in SiO₂ (i.e. nonbridging oxygen hole center) [8]. In fact, our Rutherford backscattering studies on Ge ion-implanted SiO₂ (thermally grown) samples showed that implanted and annealed SiO₂ layers are oxygen deficient,

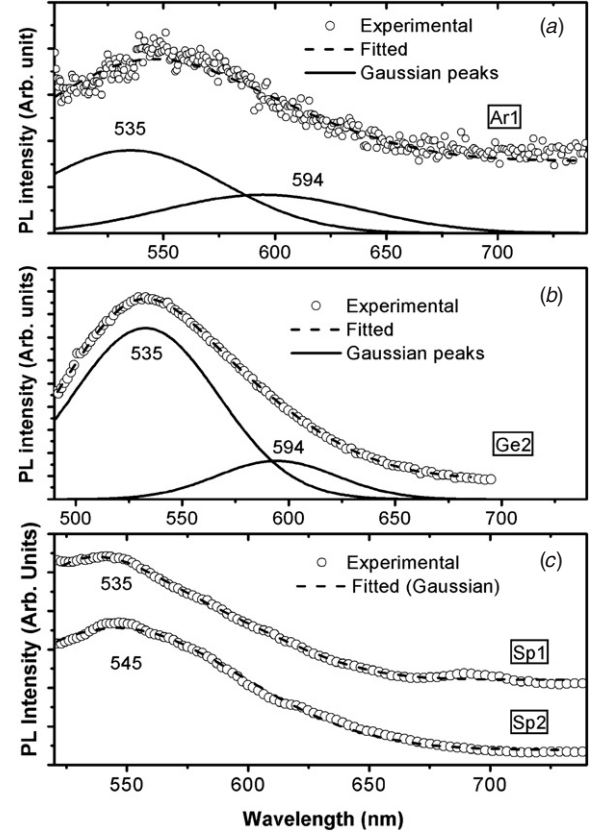


Figure 5. Room temperature PL spectra of samples: (a) Ar1, (b) Ge2, (c) Sp1, and (c) Sp2 with laser excitation at $\lambda_{ex} = 488.0$ nm. For Ar1, Sp1 and Sp2, the peak intensity is relatively low. Constituent peaks are fitted (solid lines) with Gaussian line shape to the experimental data (symbols). Center of each peak is denoted in nm unit.

i.e. it is SiO_x, where $x < 2$. Hence, we attribute the broad visible band, shown in figure 5, to oxygen deficient defects in the SiO_x matrix. In particular, the 535 nm peak may be attributed to oxygen hole center defect in SiO_x, and the 594 nm peak may be attributed to a structural disorder in the SiO_x matrix. The oxygen content and quality of SiO_x is likely to be different in samples prepared by process I and process II, and hence a slight variation of emission intensity and peak position is reasonable. We note that there is a small change in mean position of PL emission in samples Sp1 and Sp2. This is due to different annealing conditions for these two samples and the changes in the quality of SiO_x may be responsible for such a small change.

To investigate further the contribution of defects in the PL emission, all the samples are studied with 325 nm laser excitation under identical conditions. Figure 6 shows the PL spectra excited with 325 nm for samples Ar1, Ge2, Sp1, and Sp2. We observe several additional PL peaks in the UV and violet-blue region with 325 nm excitation, in addition to a broad peak (low intensity) in the visible region (~ 514 nm). Figure 6 shows that sample Ar1 has emission peaks at 343 nm and 399 nm, sample Ge2 has peaks at 342 nm, 356 nm, 377 nm and 398 nm, sample Sp1 has peaks at 375 nm (broad), 377 nm, 409 nm, and sample Sp2 has peaks at 361 nm, 369 nm and 400 nm. Thus, the ~ 400 nm peak is common to all the samples including Ar1, where Ge atoms are not present in the SiO_x matrix. Similarly, peak at near ~ 370 nm is common

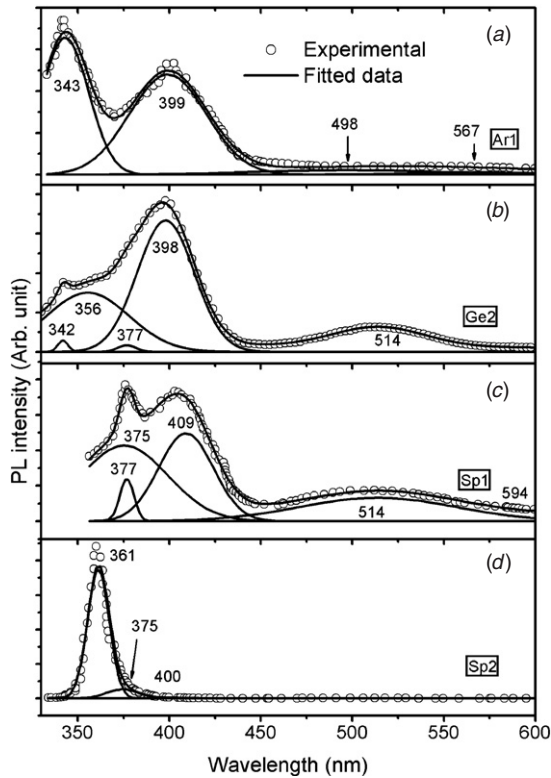


Figure 6. Room temperature PL spectra (symbols) of samples: (a) Ar1, (b) Ge2, (c) Sp1, and (d) Sp2 recorded with a 325 nm excitation. Multiple peaks are fitted (solid lines) with Gaussian line shape and center of each peak is denoted with numbers in nm. The peak at ~ 400 nm is common to all the samples.

to all SiO_x samples containing Ge atoms. Note that relative intensity of various peaks changes in different samples as a result of different processing conditions. For example, the 377 nm peak is very strong in the Sp1 sample that has been annealed at lower temperature compared to that of Ge2 and Sp2. It may be noted that Liao *et al* observed a PL emission peak at 370 nm with UV excitation in Si-implanted SiO_2 as well as in unimplanted SiO_2 , and they suggested it to be an intrinsic defect in the SiO_x matrix. Thus, the observed peaks at 377 nm and 400 nm may not be specific to Ge-related defects in the SiO_x matrix. Rather, it should be related to the oxygen deficient Si-Si or Si-Ge defects in the SiO_x matrix [9] and properties of these defects are not specific to particular atomic species in SiO_x , but specific to the local variation of defect potential caused by various atomic species [13]. Raman modes observed at 445 cm^{-1} and 420 cm^{-1} in Sp1 and Sp2 samples, respectively, are signature of such defects in the SiO_x matrix. Rebohle *et al* suggested that in the case of neutral oxygen vacancies in SiO_x , for a transition from triplet T_1 state to singlet S_0 state, one would expect a blue shift of the PL peak position with the substitution of more Ge atoms in the SiO_2 matrix. In case of Ar-implanted SiO_x matrix, nature of oxygen vacancy defects or the ODCs is expected to be different from the other samples containing Ge. Hence, the UV emission peaks are located differently. We note that intensity of 400 nm peak is negligibly low in the Sp2 sample that has been annealed at 900°C . This is due to the reduction of ODCs with high temperature annealing.

In the literature, there exists controversy regarding the origin of the ~ 400 nm peak, since some authors have attributed

it to Ge-related defects in SiO_2 or GeO_2 [14], while others have attributed it to oxygen deficient defects in the SiO_2 matrix [9, 11]. However, the present study and the reports of [12, 13] strongly suggest that the ~ 400 nm emission band is not necessarily related to Ge atoms or not specific to Si-Ge or Ge-Ge bond formation in the SiO_2 matrix. Our results suggest that some forms of ODCs in the SiO_x matrix are responsible for the 400 nm emission band. In fact, Meinardi and Paleari [13] have argued that different rearrangements of the defect environment depending on the defect (ODCs) formation processes play the key role in determining the PL features at around 400 nm. Thus the 400 nm emission band in SiO_2 is impurity species independent. In the present study, the ODCs could be formed by Si-Si bond formation in Ar-implanted samples or Si-Ge or Ge-Ge bond formation in other samples containing Ge. Similar conclusions can be drawn about the 377 nm peak, since the peak is present in all the samples. It is supported by the fact that the 377 nm peak intensity is low in Ge2 or Sp2 samples that are annealed at higher temperature and bond reconstruction takes place at higher temperature. In Sp2 samples, the ODCs are less due to higher temperature of annealing and correspondingly the 400 nm emission intensity is very low. On the other hand, in a Ge-implanted Ge2 sample, despite the annealing at 900°C , the defect concentration is relatively large due to heavy damage caused by implantation and less recovery of damage takes place during the annealing process.

It may be noted that Ge^+ -ion implantation in the SiO_x matrix followed by annealing not only induces growth of Ge NCs, but also shows formation of small Si clusters [36] in the SiO_x matrix, since the matrix is Si-rich. Therefore, presence of small amorphous Si clusters in Ar1 and Ge2 cannot be ruled out. These clusters may cause local strain in the SiO_x matrix. Lopes *et al* have shown significant presence of Ge atoms outside the NCs in the Ge-implanted SiO_2 matrix, even after 900°C annealing. The presence of substoichiometric Si oxide and defective interface between NCs and the surrounding defective matrix may cause strain in the Ge NCs. Furthermore, a lattice mismatch between Ge and Si crystallites may cause strain, since Ge-Si bond vibration with different compositions is seen from the Raman spectra of Sp1 and Sp2 samples. We believe that in the case of embedded Ge NCs, the ODCs in the oxide matrix and/or the poor quality of interface between the NCs and the defective oxide matrix dictate the photoluminescence properties of the embedded NCs. From the Raman line width analysis, we found that NCs prepared by sputter deposition are more strained than the sample prepared by ion implantation. This strain may be responsible for lower intensity of PL emission (both visible and UV peaks) from Sp1 and Sp2 samples as compared to Ge1 and Ge2 samples.

It is noteworthy that despite the presence of well-formed spherical Ge NC in these samples or those reported in the literature, visible PL could not be related to the radiative recombination of excitons confined in the Ge NCs. Ge NCs in the diameter range 6–13 nm are expected to show a quantum size effect, since the excitonic Bohr radius in Ge is about 17.7 nm. However, all the PL emission bands in the UV to visible regions are related to defects in the oxide matrix and even the near IR PL has been reported to be

due to defects. We believe that the absence of PL emission related to the quantum confinement effect is primarily related to the strain field in the interior of the small NCs and the unavoidable surface defects at the NCs that are embedded in the SiO_x matrix. The strain field may act as a nonradiative recombination channel for the NCs and the expected PL due to quantum-confined excitons is perhaps quenched by the nonradiative defects. Another possibility is that photoexcited carriers may prefer to recombine at the ODC sites or at the NC/ SiO_x interface and sufficient carriers may not be available for the band-to-band recombination. This may be the reason why no PL emission has been unambiguously attributed to recombination at the core of the NCs. We conjecture that choosing a different embedding matrix other than SiO_x may circumvent this problem and for a strain-free Ge NC, expected enhancement in the PL efficiency of Ge NCs may become a reality. More studies would be required in this direction.

4. Conclusion

In conclusion, comparative studies on embedded Ge NCs formed by sputter deposition and ion-implantation techniques show that Ge NCs in the size range 6–13 nm are formed embedded in SiO_x matrix of different samples. Optical Raman studies strongly indicate the presence of strain in the Ge NCs. LFRS studies show only surface symmetrical acoustic phonon modes of Ge NCs in implanted samples, whereas sputter-deposited NCs show surface symmetrical and surface quadrupolar acoustic phonon modes. PL studies with different excitation wavelengths show that the entire range of visible and UV PL emissions primarily originates from oxygen deficient defects in the SiO_x matrix, and properties of these defects are less specific to impurity atom species. It is proposed that the light emission due to radiative recombination of excitons confined in Ge NCs is inhibited due to the inherent strain in the embedded NCs and growth of unstrained Ge NCs in a non-oxide matrix may allow one to observe the expected visible PL emission from small Ge NCs.

Acknowledgments

We thank Sidananda Sarma for help in the XRD measurements. Financial support from DAE, BRNS to carry out part of this work is gratefully acknowledged. SB acknowledges the financial support from UGC-DAE toward research fellowship.

References

- [1] Min K S, Shcheglov K V, Yang C M, Atwater M A, Brongersma M L and Polman A 1996 *Appl. Phys. Lett.* **68** 2511
- [2] Wu X L, Gao T, Siu G G, Tong S and Bao X M 1999 *Appl. Phys. Lett.* **74** 2420
- [3] Maeda Y 1995 *Phys. Rev. B* **51** 1658
- [4] Takeoka S, Fujii M, Hayashi S and Yamamoto K 1998 *Phys. Rev. B* **58** 7921
- [5] Singha A, Roy A, Kabiraj D and Kanjilal D 2006 *Semicond. Sci. Technol.* **21** 1691
- [6] Torchynska T V, Aguilar-Hernandez J, Schacht Hernández L, Polupana G, Goldstein Y, Many A, Jedrzejewski J and Kolobov A 2003 *Microelectron. Eng.* **66** 83
- [7] Das K, Goswami M N, Mahapatra R, Kar G S, Dhar A, Acharya H N, Maikap S, Lee J-H and Ray S K 2004 *Appl. Phys. Lett.* **84** 1386
- [8] Kartopua G, Bayliss S C, Hummel R E and Ekinici Y 2004 *J. Appl. Phys.* **95** 3466
- [9] Rebohle L, von Borany J, Yankov R A, Skorupa W, Tyschenko I E, Fröb H and Leo K 1997 *Appl. Phys. Lett.* **71** 2809
- [10] Skorupa W, Yankov R A, Rebohle L, Frob H, Bohme T, Leo K, Tyschenko I E and Kachurin G A 1996 *Nucl. Instrum. Methods B* **120** 106
- [11] Sahoo P K, Dhar S, Gasiorek S and Lieb K P 2004 *J. Appl. Phys.* **96** 1392
- [12] Liao L S, Bao X M, Zheng X Q, Li N S and Min N B 1996 *Appl. Phys. Lett.* **68** 850
- [13] Meinardi F and Paleari A 1998 *Phys. Rev. B* **58** 3511
- [14] Zacharias M and Fauchet P M 1997 *Appl. Phys. Lett.* **71** 380
- [15] Kanimetsu Y, Uto H, Masumoto Y and Maeda Y 1992 *Appl. Phys. Lett.* **61** 2187
- [16] Cheung A, Azevedo G de M, Glover C J, Llewellyn D J, Elliman R G, Foran G J and Ridgway M C 2004 *Appl. Phys. Lett.* **84** 278
- [17] Choi W K, Chew H G, Zheng F, Chim W K, Foo Y L and Fitzgerald E A 2006 *Appl. Phys. Lett.* **89** 113126
- [18] Wellner A, Paillard V, Bonafos C, Coffin H, Claverie A, Schmidt B and Heinig K H 2003 *J. Appl. Phys.* **94** 5639
- [19] Wu X L, Gao T, Bao X M, Yan F, Jiang S S and Feng D 1997 *J. Appl. Phys.* **82** 2704
- [20] Sharp I D, Xu Q, Yi D O, Yuan C W, Beeman J W, Yu K M, Ager J W III, Chrzan D C and Haller E E 2006 *J. Appl. Phys.* **100** 114317
- [21] Duval E, Boukenter A and Champagnon B 1986 *Phys. Rev. Lett.* **56** 2052
- [22] Teo K L, Kwok S H, Yu P Y and Guha S 2000 *Phys. Rev. B* **62** 1584
- [23] Fujii M, Nagareda T, Hayashi S and Yamamoto K 1991 *Phys. Rev. B* **44** 6243
- [24] Tanaka A, Onari S and Arai T 1993 *Phys. Rev. B* **47** 1237
- [25] Lamb H 1882 *Proc. London Math.* **13** 189
- [26] Cheng W, Ren S and Yu P Y 2003 *Phys. Rev. B* **68** 193309
- [27] Giri P K, Kesavamoorthy R, Panigrahi B K and Nair K G M 2005 *Solid State Commun.* **136** 36
- [28] Yang Y M, Yang L W and Chu P K 2007 *Appl. Phys. Lett.* **90** 081909
- [29] Alosno M I and Winer K 1989 *Phys. Rev. B* **39** 10056
- [30] Richter H, Wang J P and Ley L 1981 *Solid State Commun.* **39** 625
Campbell I H and Fauchet P M 1986 *Solid State Commun.* **58** 739
- [31] Das K, Goswami M N L, Dhar A, Mathur B K and Ray S K 2007 *Nanotechnology* **18** 175301
- [32] Lopes J M J, Zawislak F C, Behar M, Fichtner P F P, Rebohle L and Skorupa W 2003 *J. Appl. Phys.* **94** 6059
- [33] Yadav H K, Gupta V, Sreenivas K, Singh S P, Sundarakannan B and Katiyar R S 2006 *Phys. Rev. Lett.* **97** 085502
- [34] Ovsyuk N N, Gorokhov E B, Grischenko V V and Shebanin A P 1988 *JETP Lett.* **47** 298
- [35] Giri P K, Kesavamoorthy R, Panigrahi B K and Nair K G M 2005 *Solid State Commun.* **133** 229
- [36] Giri P K, Kesavamoorthy R, Bhattacharya S, Panigrahi B K and Nair K G M 2006 *Mater. Sci. Eng. B* **128** 201

Queries

- (1) Author: Please check the term 'up shift' here and elsewhere in the text. Should it be 'upward shift'?
- (2) Author: Please check whether the journal title in reference [33] is correct as set.

Reference linking to the original articles

References with a volume and page number in blue have a clickable link to the original article created from data deposited by its publisher at CrossRef. Any anomalously unlinked references should be checked for accuracy. Pale purple is used for links to e-prints at arXiv.